ELSEVIER

Journal of Hydrology 267 (2002) 244–257

Journal of Hydrology

www.elsevier.com/locate/jhydrol

Three-dimensional imaging of pore water diffusion and motion in porous media by nuclear magnetic resonance imaging

Karl-Heinz Herrmann[a,*], Andreas Pohlmeier[a], Daniel Gembris[b], Harry Vereecken[a]

[a]*Research Center Jülich, ICG-IV, D-52425 Jülich, Germany*
[b]*Research Center Jülich, IME, D-52425 Jülich, Germany*

Abstract

We report on the use of a pulsed gradient spin-echo imaging sequence for the three-dimensional (3D) imaging of water transport properties in two porous media: 2 mm glass-beads and 0.15 mm quartz-sand mixed with 2 mm glass-beads. In contrast to tracer methods, which monitor the tracer motion by its effect on the signal relaxation of ^{1}H, this sequence measures the echo signal intensity I_0 without and I with applied diffusion gradient, respectively. For the wide-pore glass-bead system, the intensity loss is controlled by nearly free self-diffusion in the pores. A mean apparent diffusion coefficient is calculated from the ratio $\ln(I_0/I)$ as $\langle D_{\mathrm{loc}}\rangle = 1.9\times10^{-9}$ m^2 s^{-1}, which is slightly lower than that of free water ($D = 2.3\times10^{-9}$ m^2 s^{-1}). Increasing the mean pore flow velocity from 0 to 0.14 mm s^{-1} results in a linear increase of $\langle D_{\mathrm{loc}}\rangle$ to 2.3×10^{-9} m^2 s^{-1}, caused by mechanical dispersion. The spatial distribution is of the log-normal type, where the width increases with increasing pore velocity. Correlation lengths are also calculated.

For the fine porous medium, frequent contacts of the water molecules with the pore boundaries lead to a significant decrease of I_0 by increased T_2 relaxation. The resulting ratio of the signal intensities $\ln(I_0/I)$ is then smaller than expected for pure diffusion, which is caused by the restricted diffusion in the fine pore system. The spatial distribution (normal) is broader than for the glass-bead system and the mean local apparent diffusion coefficient is calculated as 1×10^{-9} m^2 s^{-1}, a dependence on the pore flow velocity could not be detected.

For the glass-bead system, the 3D image clearly shows regions of increased dispersivity (50% greater than the $\langle D_{\mathrm{loc}}\rangle$), caused by packing errors, leading to preferential flow. This macroscopic effect on the column scale is quantified by a numerical simulation of tracer transport, based on the 3D diffusion coefficient field, assuming a linear relation to local velocities. From this simulation, the effective dispersion coefficient is obtained for the column scale ($D_{\mathrm{eff}} = 130\times10^{-9}$ m^2 s^{-1}), which is comparable to that obtained from classical break-through curves with tracer substances. © 2002 Published by Elsevier Science B.V.

Keywords: Magnetic resonance imaging; Porous media; Velocity distribution; Correlation length; Diffusion coefficient; Dispersion

1. Introduction

The soil belongs to the most important sink of contaminants in the terrestrial environment. Physically, it is a porous medium, composed of a solid matrix of various inorganic and organic substances, a fluid phase, which is an aqueous electrolyte solution of various solutes, and, under unsaturated conditions, of air. A considerable amount of knowledge about transport processes has been gained in the past by black-box methods and models, i.e. the internal structure of the porous medium is (necessarily) parameterized by empirical parameters like porosity, water content, hydraulic conductivity, affinity of the solute to the solid matrix, etc. Combining one-dimensional (1D) experiments like break-through curves with 1D models, a forecast of the fate of

* Corresponding author.
E-mail address: k.-h.herrmann@fz-juelich.de (K.H. Herrmann).

0022-1694/02/$ - see front matter © 2002 Published by Elsevier Science B.V.
PII: S0022-1694(02)00154-3

contaminants has been tried. However, this approach is of rather limited value, since the processes in the interior are not observable directly without destroying the structures and they will yield no insight into possibly complex processes in the interior that lead to the macroscopically observed parameters. Due to these problems, the application of non-invasive techniques for the monitoring of water flow and solute transport properties of porous media are of great interest for gaining new information about transport processes in soils. With the nuclear magnetic resonance imaging technique (NMRI), a powerful instrument is available for a detailed, high-resolution 3D characterization of transport properties in porous media.

The application of MRI to the study of porous media is subject of many new publications. Generally, one has to differentiate between (i) tracer methods, which monitor the effect of a paramagnetic tracer substance on the MR response and (ii) methods which observe the water diffusion and motion directly. Each of these approaches has its own advantages, and their respective application fields and limitations are a challenging new area of research, which is developing rapidly.

(i) For instance, the group of Kinzelbach (Oswald et al., 1997) has employed MRI for the monitoring of a tracer (Cu^{2+}) in an artificial sandy porous medium. They found even for a homogeneous medium complicated flow patterns in form of a fingering. Grenier et al. (1997) demonstrated that the convective and dispersive transport could be visualized in saturated porous media consisting of 0.5 mm glass-beads by using MRI and they subsequently derived transport parameters from the observed data.

(ii) Some examples for the direct observation of flow properties are given in the review of Watson and Chang (1997). The group of Berkowitz employed a direct velocity sensitive spin-echo sequence for the monitoring of high velocities in fractured systems (Dijk et al., 1999; Dijk and Berkowitz, 1999), and Sederman and Gladden (2001) have also visualized the flow directly in a system of 5 mm glass-beads for velocities up to 9 mm s^{-1}. Scheenen et al. (2001) could image apparent diffusion coefficients in maize plants, and Baumann et al. (2000) have monitored the water flow in media of different porosity by use of an EPI sequence. The application of diffusion sensitive pulsed gradient sequences on porous media is reported by Manz et al. (1999) and De Panfilis and Packer (1999) for the investigation of dispersive processes in porous media.

The purpose of this investigation is to image the 3D field of local diffusion coefficients, to analyze their spatial correlation and to detect areas of increased permittivity. In contrast to our previously published investigations (Herrmann et al., 2002), where the tracer motion was observed, this study is focused on the use of a pulsed gradient spin-echo (PGSE) method to gain insight in the transport and flow properties of water in two different porous media: homogeneous glass-beads and a mixture of quartz-sand and 20% glass-beads. The PGSE method allows a direct access to the local apparent diffusion coefficient of the water inside each of the observation volume elements, the *voxel*.[1] The local apparent diffusion coefficient is also a function of the mean flow velocity, and it may be affected by mechanical dispersion. The obtained 3D field of local diffusion coefficients will be analyzed further by statistical procedures. Finally, this information is used to simulate the tracer transport through the medium to obtain effective dispersive properties of the whole column. The nature of the local, apparent diffusion coefficients and the macroscopic effective dispersion coefficients will be discussed.

2. Theory

2.1. MRI

The nuclear magnetic resonance of the ^1H atoms (NMR) is used to measure the motion of water in the porous media under consideration by means of a PGSE sequence,[2] where the imaging is performed by echo planar imaging (Callaghan, 1991; Gembris,

[1] Voxel is used in NMRI for an elementary volume which is then represented as one data pixel in the images.

[2] The term 'PGSE' is usually restricted to NMR spectroscopy, but we extend it to MRI, where the gradient switching rates are much lower.

2001; Herrmann, 2001). A detailed description of the effect, as well as the imaging principles would exceed the frame of this work by far, so the interested reader is referred to the literature (Callaghan, 1991). The sequence yields an echo signal in each volume element of the 3D space according to:

$$I_i = I_{0,i} \exp(-\gamma^2\delta^2\Delta G^2 D_{\mathrm{loc},i} + \mathrm{i}\gamma\delta\Delta G v_i) \tag{1a}$$

where the subscript i denotes the spatial directions x, y, and z.

For convenience, the following factors are defined:

$$b = \gamma^2\delta^2\Delta G^2 \tag{1b}$$

and

$$a = \gamma\delta\Delta G \tag{1c}$$

In Eqs. (1a)–(1c), γ is the gyromagnetic ratio of ^{1}H, δ and Δ represent duration and separation of the pulsed diffusion gradients, respectively, G is the gradient pulse strength and v the local flow velocity. $D_{\mathrm{loc},i}$ is the *apparent*, *local* diffusion coefficient of water—apparent, since it contains the molecular diffusion, as well as mechanical dispersion under flow conditions in porous media, and local, since it describes the diffusive properties on the voxel scale. Setting $G = 0$ (i.e. $a, b = 0$) leads to $I_i = I_{0,i}$, the echo intensity without motion sensitivity. The employed sequence measures I_0, followed by successively applying G in the three spatial directions x, y and z to determine I_i. By analyzing the phase information, the flow velocity components of v (v_x, v_y, v_z) can be determined. The local diffusion coefficients $D_{\mathrm{loc},i}$, must not be confused with the conventional macroscopic effective dispersion coefficient D_{eff}, obtainable, e.g. by analysis of break-through curves.

2.2. Flow in porous media

In porous media, the conventional molecular diffusion is superimposed by a dispersive effect: due to the inhomogeneous flow paths of neighboring water molecules the effective dispersion coefficient D_{loc} is greater than that of undisturbed water. Therefore, $D_{\mathrm{loc},i}$ in Eqs. (1a)–(1c) comprises the self-diffusion coefficient of undisturbed water D_0 and a term, often called mechanical dispersion, depending on the pore water velocity v_{p} as stated by Pfannkuch (1963) and Roth (1996):

$$D_{\mathrm{loc},i} = D_0 + \lambda|v_{\mathrm{p}}| \tag{2}$$

where λ is the dispersivity parameter of the porous medium.

A variation of the mean pore flow velocity should results in a linear increase of $D_{\mathrm{loc},i}$ according to Eq. (2), which is confirmed by experiments (see also Fig. 2). The linear relationship between the mean pore velocity and the mean value of apparent local diffusion coefficient $\langle D_{\mathrm{loc}}\rangle$ can be used as calibration for the local velocities inside each voxel.

2.3. Statistical analysis

The obtained 3D dispersion and flow data are statistically analyzed by means of the program package GSLIB (Deutsch and Journel, 1992). A convenient measure for the spatial correlation of the local dispersion and fluxes is the covariance as defined by:

$$S(\mathbf{h}) = \frac{1}{N(\mathbf{h})}\sum_{j=1}^{N(\mathbf{h})} z(\mathbf{u}_j)z(\mathbf{u}_j+\mathbf{h}) - \bar{z}\bar{z}_h \tag{3}$$

where $S(\mathbf{h})$ is the correlation function, N is the number of regarded data pairs, z, the random variable which is analyzed ($D_{\mathrm{loc},i}$ in our case), $\mathbf{u}_j$ the position and $\mathbf{h}$ describes a defined distance from the position $\mathbf{u}_j$ into the direction under consideration. If an exponentially decaying function is obtained, the correlation length l_{corr} is defined as follows:

$$S(\mathbf{h}) = S(0)\exp(-|\mathbf{h}|/l_{\mathrm{corr}}) \tag{4}$$

The expectation values in Eq. (3) are defined as:

$$\bar{z} = \frac{1}{N(\mathbf{h})}\sum_{j=1}^{N(\mathbf{h})} z(\mathbf{u}_j) \tag{5}$$

and

$$\bar{z}_h = \frac{1}{N(\mathbf{h})}\sum_{j=1}^{N(\mathbf{h})} z(\mathbf{u}_j+\mathbf{h}) \tag{6}$$

The PGSE method can be used to determine the local dispersive properties in the porous medium, as stated in Section 2.2. In classical break-through experiments frequently an effective macroscopic dispersion coefficient D_{eff} can be determined by fitting the convective

dispersion equation (CDE) to these curves. For the derivation of a comparable quantity from our experiments (which are performed without a tracer substance), the tracer transport is simulated by the program PARTRACE (Neuendorf, 1997), based on the flow velocity field obtained from our data. Freyberg (1986) has derived an analytical expression for the relation of the effective macroscopic dispersion coefficient $D_{\mathrm{eff},y}$ to the second spatial central moment $\mu_2(C(y,t))$ of the concentration distribution $C(y,t)$ at times t of a conservative tracer, transported through the porous medium:

$$D_{\mathrm{eff},y} = \frac{1}{2}\frac{\mathrm{d}}{\mathrm{d}t}\mu_2(C(y,t)) \tag{7}$$

So from Eq. (7) $D_{\mathrm{eff},y}$ can be obtained by plotting $\mu_2(C(y,t))$ versus time and the results have been shown to be in good accordance with breakthrough curve analysis. This method provides in addition to the effective dispersion coefficient $D_{\mathrm{eff},y}$ also the range of validity in which this $D_{\mathrm{eff},y}$ does represent the mean dispersivity of the column under consideration.

3. Experimental setup

The experimental setup consists of vertically mounted PMMA columns with an inner diameter of 6 cm and a height of 18 cm. The inflow is located at the bottom to provide fully saturated conditions. It consists of a filter plate for distributing the water flow homogeneously over the whole column cross-section. The two porous media employed are (1) regular glass-beads of 2 mm diameter and (2) a mixture of 80% quartz-sand with a mean grain size of 150 μm and 20% of the glass-beads. A constant water flow through the column was generated by a chromatography pump. The MR scanner used in the experiments is a Siemens Magnetom 1.5T system designed for whole-body scans. The sample temperature was 24 °C. To increase the signal to noise ratio, we employed the standard head coil system. Since no metal parts were allowed in the vicinity of the scanner the pump was located in an adjacent room and connected with the column by two 10 m teflon tubes of (1/16) in. inner diameter.

The spatial coordinates used in this study are y for the transport direction (up in the laboratory coordinate system), x for the horizontal direction perpendicular to that (from right to left in the laboratory coordinate system), and z the direction along the axis of the whole-body scanner (from front to back in the laboratory system). The PGSE sequence has a resolution of 96×128 voxels which are interpolated (still in the Fourier space) by the control computer to either 128×128 voxels (2.25 mm × 2.25 mm) in the case of the quartz-sand and to 256×256 voxels (1.25 mm × 1.25 mm) for the glass-beads. The volume is scanned in the z-direction by a separate gradient, leading to a slice thickness of 4 mm in all cases. So the resulting voxel scale is 6 and 20 mm^3 for the glass-bead, and mixed (quartz-sand/glass-bead) system, respectively. All visualizations and constructions of *iso-surfaces* are performed by means of the program IDL.

4. Results and discussion

The validity of the magnitude term in Eq. (1a) for porous media has been checked by plotting the mean value of the signal magnitude in y-direction versus b (Eq. (1b)) for the two systems: glass-beads of 2 mm diameter and the mixed system as described in the experimental part. A linear relation has been obtained proving the validity of Eq. (1a) also for porous media. From the slopes, the mean local diffusion coefficients $\langle D_{\mathrm{loc}} \rangle$ are calculated as 1.9×10^{-9} and $1.0 \times 10^{-9}\ \mathrm{m^2\,s^{-1}}$ for glass-beads and the mixed system, respectively. These values are smaller than the diffusion coefficient of pure water in unrestricted volumes, which is determined as $2.3 \times 10^{-9}\ \mathrm{m^2\,s^{-1}}$ by applying the sequence to a columns filled only with water (literature value: $2.47 \times 10^{-9}\ \mathrm{m^2\,s^{-1}}$, Landold-Börnstein, 1969). The reason is the restricted diffusion of the water molecules in the narrow pores, which are in the case of the glass-beads the areas near the contact sites of the beads. For the fine pore system, this effect is even more pronounced. In the following, the results for the two systems will be presented separately.

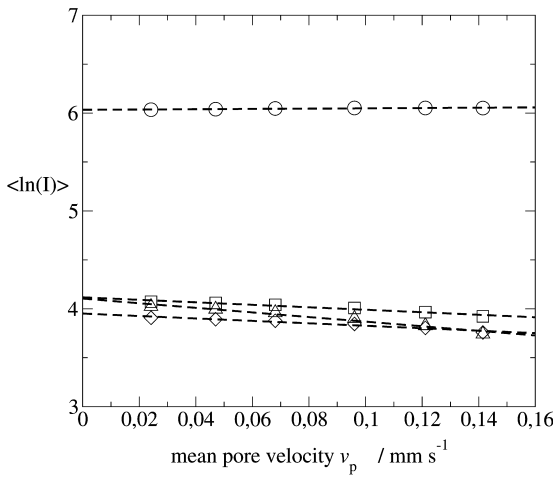

Fig. 1. Results for the glass-bead column: measured mean MR echo intensities ($\langle \ln(I_i) \rangle$) averaged over the whole column, with $b = 0$ s mm^{-2} (○) and $b = 1000$ s mm^{-2}, in direction x (◇), z (□) and transport direction y (△), as a function of the mean pore velocity.

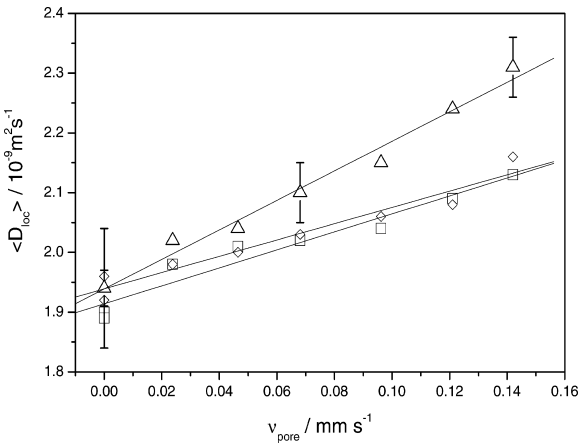

Fig. 2. Calculated mean local diffusion coefficients $\langle D_{loc} \rangle$ for the glass-bead column. Transport direction y (△), transverse directions x (◇), z (□). Errorbars for the x and z-direction are omitted for reasons of clarity. Note that for $v_p = 0$ mm s^{-1} two errorbars are shown: the small is valid for the averaging over four scans, the great for the single scan. (see Table 1).

4.1. Glass-bead column

4.1.1. Local diffusion coefficients

Fig. 1 shows the mean value of the logarithmic signal intensities in each voxel, averaged over the whole column ($\langle \ln(I) \rangle = \sum_i \ln(I_i)/N_{voxel}$), and plotted versus the mean pore velocity obtained from the applied external conditions (flux, porosity, diameter). For $b = 0$ s mm^{-2}, i.e. without diffusion (dispersion) sensitivity (curve O), $\langle \ln(I_0) \rangle$ is independent of v_p, and for $b = 1000$ s mm^{-2} $\langle \ln(I_i) \rangle$ decreases linearly with v_p for all three directions x, y and z. The linear regression lines for the y and z direction meet at $\langle \ln(I_i) \rangle = 4.10$, whereas the line for x is shifted by a constant value of 0.15 to lower values. The reason is a magnetic background gradient, induced by the filling of the column, which induces an additional decrease of the intensity in the (with respect to the length axis of the MRI scanner) transverse direction. (For details, see Zhong et al. (1991) and Gembris (2001)). This effect has been checked by recording the 3D image with swapped imaging gradients ($x \leftrightarrow y$), which also swaps the position of $\ln(I)$ data on the ordinate of Fig. 1. So this effect cannot be due to hydrodynamic properties of the porous medium, but it is caused by the different strengths of the imaging gradients in the x and y directions. So for the compensation of this effect $\ln I$ data in x-direction are shifted by 0.15. Fig. 2 shows the mean diffusion coefficients for the three spatial directions as a function of the mean flow velocity.

Two findings should be discussed here, before continuing with the analysis of the spatial distribution of the local diffusion coefficients.

(i) The local apparent diffusion coefficients $D_{loc,i}$ are in the order of magnitude of that for free water. But they are much smaller than effective dispersion coefficients obtained from breakthrough experiments. This discrepancy results from the local aspect, which is accessible by this PGSE sequence since this sequence probes the mm scale, i.e. inside one voxel. On the column scale, the effective dispersion coefficient is controlled by column scale heterogeneities, i.e. on the cm to dm scale. The imposed pore flux (0–0.14 mm s^{-1}) induces an increase of the apparent local diffusion coefficients. This effect is due to the mechanical dispersion induced by the flow in pores. The magnitude of this mechanical dispersion is small compared to the value of the diffusion coefficient of water in the pore space since the sequence probes the voxels till the echo time, which is $T_E = 100$ ms for the employed sequence, and in this time the water

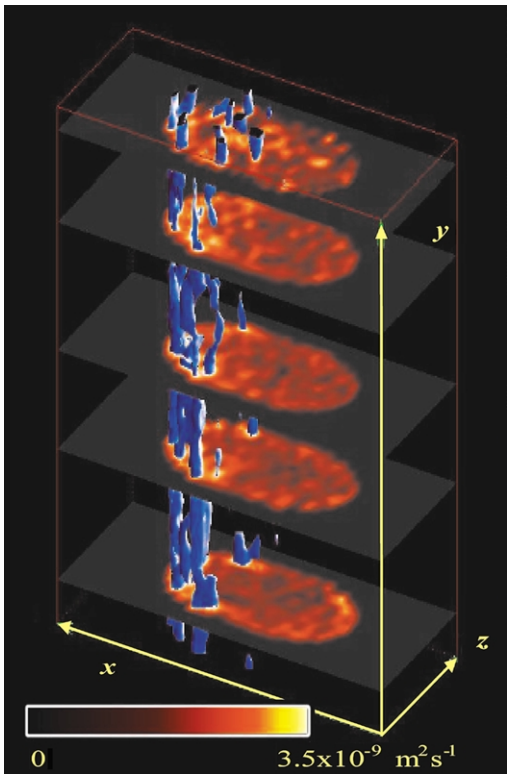

Fig. 3. Results for the glass-bead column: 3D visualization of the local diffusion coefficient field (y-component). A layer of 2 mm is already removed at the outer boundary of the column to suppress the display of the immediate wall effects. The red slices are 2D cuts through the column depicting the y-component (main flow direction along the central axis of the column) of the local diffusion coefficients. The overlayed blue surface (iso-surface) encloses all voxels with $D_{\mathrm{loc},y} > 2.9 \times 10^{-9}$ m^2 s^{-1} for a mean flow rate of 0.142 mm s^{-1}.

molecules do not move over more than one pore diameter even at the highest flux. At this flux, the mean advective displacement is 0.014 mm and the mean diffusional displacement is $\langle R \rangle = (6D_{\mathrm{loc},y}t)^{1/2} = 0.056$ mm in 100 ms, both distances are much smaller than the pore size of the 2 mm glass-bead medium. The measured apparent diffusion coefficient registers flow path differences within the voxel and cannot comprise large-scale flow differences like preferential flow paths on the column scale.

(ii) While increasing the mean pore water velocity, the y-component of D_{loc} (- -△- -△- -) increases stronger than the x- and z-component indicating a stronger influence of the mechanical (i.e. flow induced) dispersion on the local diffusion coefficient in the transport direction. This agrees qualitatively with the well-known dispersion behavior in porous media (De Marsily, 1986), but the slopes differ only approximately by a factor of 2, which is rather small compared to Marsily, who states a factor of 5–100. We have verified that this effect is not caused by different sensitivities in the three directions of the MR system, but by the short distances probed by our experimental setup, whereas Marsily's results are valid for longer transport distances.

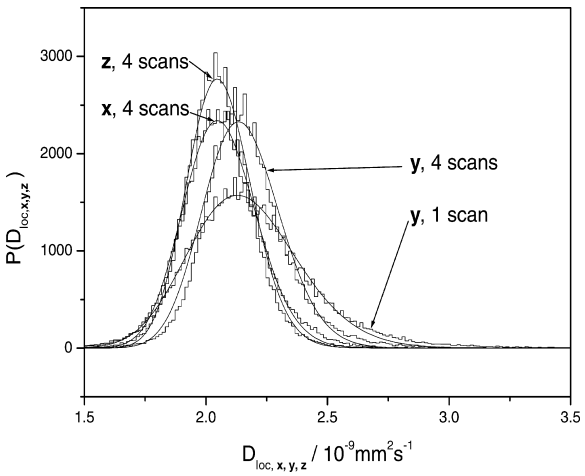

Fig. 4. Local diffusion coefficient distributions in the glass-bead column for a mean pore velocity $v_{\mathrm{p}} = 0.096$ mm s^{-1}. P(D) denotes bin counts. Shown are the results for the three spatial directions (x, z, and y = transport) as histograms. Additionally the histogram of the distribution of a single scan is presented. Curved lines are fits with a log-normal distribution, the fitted parameters are given in Table 1.

Summarizing the results obtained so far, it can be stated that the mean values of the x, z, and y (transport direction) components of the local diffusion coefficient D_{loc} on the voxel scale are valid for short distances and time of water movement through the porous medium. Even at this small scale, where the mean travel length is in the order of magnitude of the pore diameter, an influence of the heterogeneous flow trajectories is measurable, resulting in a linear increase of the

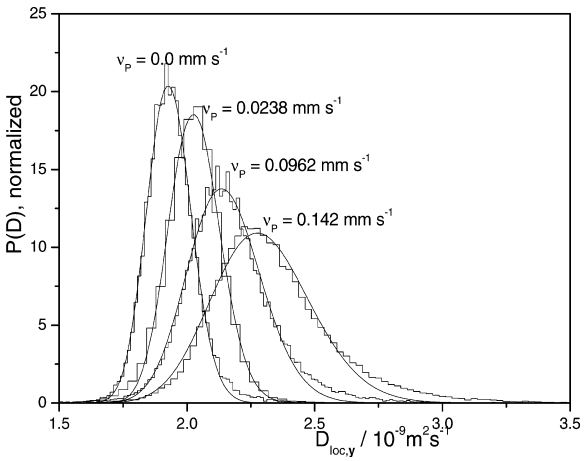

Fig. 5. Results for the glass-bead column: local diffusion coefficients distributions for four chosen (of nine available) mean pore velocities $\langle v_p \rangle$. Shown are the results for the transport direction y as histograms and fits with a log-normal distribution. Fitted parameters are given in Table 1.

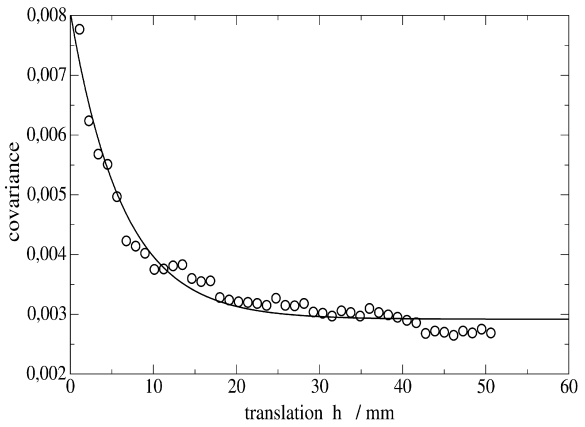

Fig. 6. Results for the glass-bead column: correlation function $S(\mathbf{h})$ according to Eq. (3) for the D_{loc} in transport direction y. The resulting correlation length in transport direction, obtained by a fit of Eq. (4) (solid line), is 7 mm.

mean local diffusion coefficient. We term this quantity as 'diffusion' coefficient, since it is mainly controlled by the self-diffusion of the water molecules (in restricted space), plus a minor contribution of the mechanical dispersion, induced by the heterogeneous flux (advection). $D_{loc,i}$ must not be confused with the classical dispersion coefficient, $D_{eff,i}$.[3] The purpose of the following investigation is to image the 3D field of local diffusion coefficients, to analyze their spatial correlation and to detect areas of increased permittivity. So the link between the local and the macroscopic dispersive properties will be made by a computer simulation, as shown later. Next, the local diffusion coefficients are analyzed statistically.

4.1.2. Statistical properties glass-bead column

Fig. 3 shows five cross-sections between 20 and 132 mm from the bottom of the column, where the colors encode the local diffusion coefficients in transport direction, $D_{loc,y}$, according to the scale at the bottom of the figure. Overlayed is a blue 'iso-surface' with a threshold value of $D_{loc,y} = 2.9 \times 10^{-9}$ m^2 s^{-1}, i.e. the blue structures enclose all volume elements, where $D_{loc,y}$ is $\geq 2.9 \times 10^{-9}$ m^2 s^{-1}. It is clearly visible that over most areas $D_{loc,y}$ varies in a limited range, but that on the left side of the column areas with a high permittivity occur (the relation between $D_{loc,y}$ and the hydraulic conductivity will be discussed later).

The distributions of the local diffusion coefficients D_{loc} for all three spatial directions x, z and the transport direction y with a mean flow rate of 0.096 mm s^{-1} are plotted in Fig. 4 in terms of a histogram. The data are obtained by averaging over four scans for each direction. Additionally, the distribution for a single scan of the y (transport) direction is shown. All distributions are fitted by a log-normal distribution (curves), yielding the mean values $\langle D_{loc,i} \rangle$ and widths σ as shown in Table 1. The log-normal distribution describes the data for the x- and z-directions (vertically to the transport) satisfactorily, but for the transport direction y especially at values for $D_{loc} > 2.5 \times 10^{-9}$ m^2 s^{-1} the log-normal distribution underestimates the local diffusion coefficients. This range represents the contribution from the areas with high diffusivity, i.e. the blue colored iso-surfaces on the left part of the column, shown in Fig. 3. This effect is also strongly dependent on the mean applied flow rate as shown in Fig. 5. The deviations of the distributions of D_{loc} in transport directions, $D_{loc,y}$, from the log-normal distributions increases with increasing flow rates.

Before continuing we want to remark the following: in Fig. 4, the increase of the number of scans from

[3] This quantity is termed *dispersion*, since this is the superior property. *Diffusion* is more special, it means irregular Brownian motion, induced by strikes of the molecules to each other. A synonym in this case is *self-diffusion*.

Table 1
Parameters of the fitted log-normal distributions for the local diffusion coefficients for four selected pore flow velocities. The data are obtained by averaging over four scans, if not marked otherwise. The errors are the uncertainty of the mean values

System	v_p (mm s^{-1})	Direction	$\langle D_{loc,i} \rangle$ ($\times 10^{-9}$ m^2 s^{-1})	σ ($\times 10^{-9}$ m^2 s^{-1})
Glass-beads (measured in Düsseldorf)	0.0	y, 10 scans	1.94 ± 0.03	0.139
		y, single scan	1.9 ± 0.1	0.32
		x	1.96 ± 0.05	0.072
		z	1.89 ± 0.05	0.086
Glass-beads	0.024	y	2.02 ± 0.05	0.11
		y, single scan	2.1 ± 0.1	0.29
		x	1.98 ± 0.05	0.12
		z	1.97 ± 0.05	0.097
Glass-beads	0.096	y	2.14 ± 0.05	0.15
		y, single scan	2.1 ± 0.1	0.21
		x	2.05 ± 0.05	0.14
		z	2.05 ± 0.05	0.13
Glass-beads	0.142	y	2.28 ± 0.05	0.18
		x	2.13 ± 0.05	0.16
		z	2.13 ± 0.05	0.14
Glass-bead/quartz-sand	0.0	y	1.0 ± 0.2	0.50
		z	0.9 ± 0.2	0.45
		x	1.1 ± 0.2	0.55
Glass-bead/quartz-sand	0.142	y	1.0 ± 0.2	0.65
		z	0.9 ± 0.2	0.60
		x	1.0 ± 0.2	0.65

1 to 4 reduces σ from 0.21×10^{-9} to 0.15×10^{-9} m^2 s^{-1}. A similar reduction is observed, increasing the number of scans from 1 to 10 for the pore velocity of 0 mm s^{-1} (Table 1, first and second line, $D_{loc,y}$). This reduces σ from 0.32×10^{-9} to 0.139×10^{-9} m^2 s^{-1}. Regarding the $1/\sqrt{(n-1)}$ law, a reduction to 0.108×10^{-9} m^2 s^{-1} would be expected, which is more narrow than obtained. The difference results from the natural heterogeneity.

The last statistical analysis performed with the data is the calculation of the correlation lengths of $D_{loc,y}$ by means of Eq. (3). As an example, Fig. 6 shows the covariance of $D_{loc,y}$ for the glass-bead column. The correlation function is satisfactorily described by Eq. (4), yielding a correlation length in transport direction of 7 mm. The transverse correlations lengths are both 4 mm (Herrmann, 2001, plots are not shown here). Keeping in mind that the correlation lengths are defined as the length, where the correlation has decreased to $1/e$ of their original value, these data imply that the correlation persists over more than 28 mm (four times the correlation length) in transport direction and more than 16 mm perpendicular to that, in other words: more than 10 and 5 bead diameters, respectively. This also reflects the existence of the long range, tube-like high-diffusivity structures, visible in the left part of the column (see Fig. 3).

3.1.3. Velocity field, simulation and effective dispersion coefficient

For the simulation of a tracer transport in the investigated medium, which will yield the mean effective dispersion coefficient for the column, a divergence free flow velocity field is necessary (Neuendorf, 1997; Seidemann, 1997). Since the local diffusion coefficients data (and the simultaneously recorded local flow velocity data contribution from the second exponential term in Eqs. (1a)–(1c) are too noisy to fulfill this condition, we apply following procedure to obtain a divergence free flow velocity field:

(i) We found a linear dependence of the mean local diffusion coefficient on the mean applied flow rate, as shown in Fig. 2.
(ii) So we calculate an apparent flow field based on

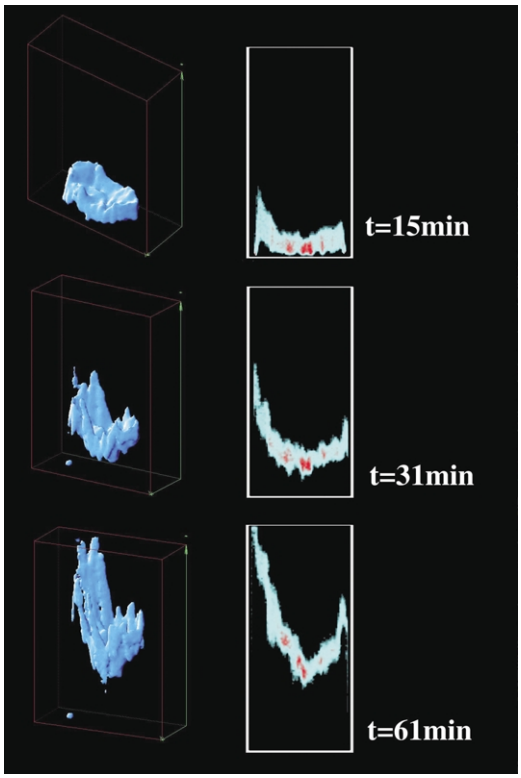

Fig. 7. The results of a tracer experiment in the glass-bead column simulated with the programs TRACE and PARTRACE (see text for details). The left part shows an iso-concentration surface enclosing all voxels with >10% of the applied tracer concentration. The right part shows the tracer concentrations for a vertical cross-section ($x-y$ plane) through the middle of the column (color coding is blue–green–yellow–red for increasing tracer concentration).

the linear relation between $D_{\mathrm{loc},y}$ and $v_{\mathrm{loc},y}$ and further assume a direct proportionality between the local flow velocities and the local values for the hydraulic conductivity κ_{loc} in case of a constant pressure gradient, i.e.

$$\kappa_{\mathrm{loc}} = \mathrm{const} \times v_{\mathrm{loc},y} = \mathrm{const}' \times (D_{\mathrm{loc},y} - D_{v=0}) \tag{8}$$

The empirical weighting factor const′ is obtained by the additional boundary condition that the overall net flux must be equal to the applied total flux of, e.g. 0.046 mm s^{-1}.

(iii) We take this 3D-κ_{loc} field as input for the program TRACE (Seidemann, 1997), which calculates a 3D flow field by solving the Richards equation in the 3D space under appropriate boundary conditions. The weighting factor is simply determinable, since the total flow calculated by TRACE must be equal to the applied total flow, known from the experimental conditions.

(iv) Based on this divergence free flow field, the program PARTRACE follows the motion of non-reactive particles in this field.

We are conscious of the approximate nature of this procedure, however, for low flow velocities no other way exists to obtain the necessary 3D flow velocity field with a precision sufficient for such model calculations with low flow velocities. The general validity of this approach has been stated already by Baumann et al. (2000). For higher local flow velocities other direct MRI methods exist to obtain the flow field (Watson and Chang, 1997; Sederman and Gladden, 2001), but the problem remains to obtain a divergence free field. An important improvement would be the use of dedicated NMR scanners with a smaller core space, stronger main magnetic field, and higher and faster gradients.

Fig. 7 shows the simulated transport of an arbitrary conservative tracer in the glass-bead column in terms of three snapshots at three different times after the isotropic injection at the bottom of the column. The right part of Fig. 7 shows cross-sections through the column, where the tracer concentration increases from blue over yellow to red. The left part of Fig. 7 represents the corresponding iso-surfaces, enclosing 90% of the total amount of tracer. The simulation shows clearly the enhanced transport velocity in the left part of the column along the high-diffusivity structures (see also Fig. 3). The mean transport rate corresponds to the mean applied flow velocity of 0.046 mm s^{-1}. The last analysis performed with the data is the calculation of the second spatial moment of the tracer distribution in the column as shown in Fig. 8. According to Eq. (7), one obtains a linear relation after a mean flow time of 25 min. The flow distance necessary to reach this Fickian flow regime in a porous medium consisting of 2 mm glass-beads, is approximately 6 cm, beyond which an effective dispersion coefficient of $D_{\mathrm{eff},y} = 130 \times 10^{-9}$ m^2 s^{-1} is established. This result for D_{eff} coincides with results obtained from conventional break-through curves for a very similar system ($D_{\mathrm{eff},y} = 93 \times 10^{-9}$ m^2 s^{-1}, see Herrmann et al.

Table 2
Summary of the hydrodynamic properties of the porous media

	l (mm)	d (mm)	v_{max} (mm s^{-1})	θ	Grain size (mm)	$D_{eff,sim}$ (10^{-9} m^2 s^{-1})	$D_{eff,tracer}$ (10^{-9} m^2 s^{-1}) (Herrmann et al. (2002))	P_e	$p_{e,approx}$	$D_{loc,y}$ (10^{-9} m^2 s^{-1})
Glass-beads	180	60	0.142	0.40	2–3	130	93	196	70	1.9
Quartz-sand/glass-beads	180	60	0.142	0.40	0.15/2				7	1.0

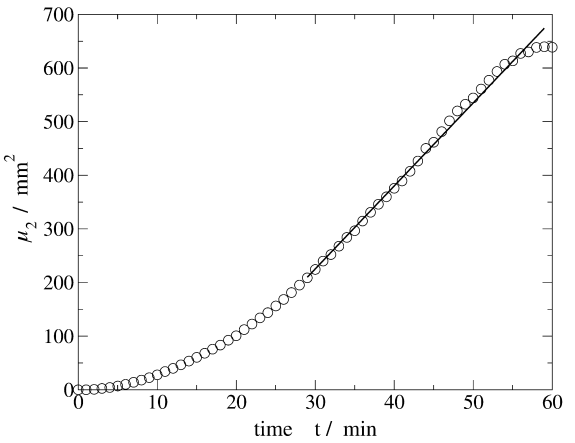

Fig. 8. Results for the glass-bead column: the second spatial central moment μ_2 of the tracer concentration in the PARTRACE simulation is plotted against time. The slope is proportional to the macroscopic effective dispersion coefficient D_{eff}. The dispersion coefficient tends to a constant slope after a time of 25 min. At 60 min some of the tracer substance already leaves the column and the spatial moment decreases again, so the slope is only meaningful up to that point.

(2002)). This simulation illustrates clearly that not the local dispersive effects control the overall effective dispersion coefficient, but the large-scale structural inhomogeneities. MRI is a powerful technique for a direct experimental observation of this effect. The hydrodynamic conditions and results are summarized in Table 2. The obtained macroscopic Peclet number $P_e = 196$, as well as the approximated microscopic Peclet number $p_e \cong 70$ reflect the convection dominated flow.

4.2. Quartz-sand/glass-bead column

4.2.1. Local dispersion

For the investigation for the effect of a porous medium with increased heterogeneity a mixture of 80% quartz-sand and 20% glass-beads is used. Like for the pure glass-bead system first the intensities of the images aquired with $b = 0$ s mm^{-2} and $b = 1000$ s mm^{-2} are averaged over all voxels inside the column and plotted in Fig. 9 versus the mean applied flux. Two effects are striking:

(i) the absolute average intensity $\langle \ln I \rangle$ at $b = 0$ s mm^{-2} decreases linearly with the mean flow velocity, whereas for the glass-bead system no change is observed (Fig. 1).

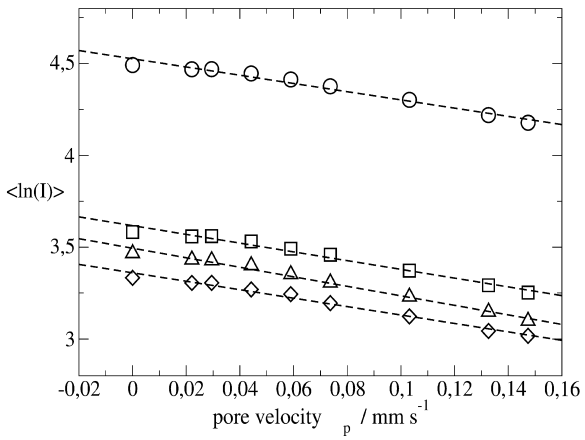

Fig. 9. Results for the mixed glass-bead/quartz-sand sample: measured mean MR echo intensities averaged over the whole column, with $b = 0$ s mm^{-2} (○) and $b = 1000$ s mm^{-2}, in direction x (◇), z (□) and transport direction y (△), as a function of the mean pore velocity.

(ii) The slopes of the diffusion weighted data, i.e. $\langle \ln I_{b=1000} \rangle$ for $b = 1000$ s mm^{-2}, are within the experimental error identical to the unweighted data ($b = 0$ s mm^{-2}).

Since according to Eqs. (1a)–(1c), the mean local diffusion coefficients are calculated as $\langle D_{\mathrm{loc}} \rangle = 1.0 \times 10^{-9}$ and 0.9×10^{-9} m^2 s^{-1} for the transport direction y (△) the transverse direction z (□), respectively. The differences $\langle \ln I_{b=0} - \ln I_{b=1000} \rangle$ for the other transverse direction is slightly greater due to the magnetic gradient, induced by the porous medium (Gembris, 2001). An increase of the mean local diffusion coefficients with the mean pore flow velocity, as found for the glass-bead system cannot be observed with the given experimental setup, since the variance of the data is too great (see also Fig. 10).

The lower absolute values (compared to the pure glass-bead system) of $\ln I_{b=0}$ and their decrease with increasing mean pore velocity can be ascribed to the loss of magnetization by frequent wall contacts during the echo time of 0.1 s: The molecular diffusion length $\langle R \rangle = (6Dt)^{1/2} = 0.025$ mm is of the same magnitude as the pore dimensions for the mixed system. Therefore, many ^1H_2O molecules in a pore will get close to a matrix surface either by diffusion or by advection, where localized magnetic gradients due to the susceptibility differences between the matrix and the

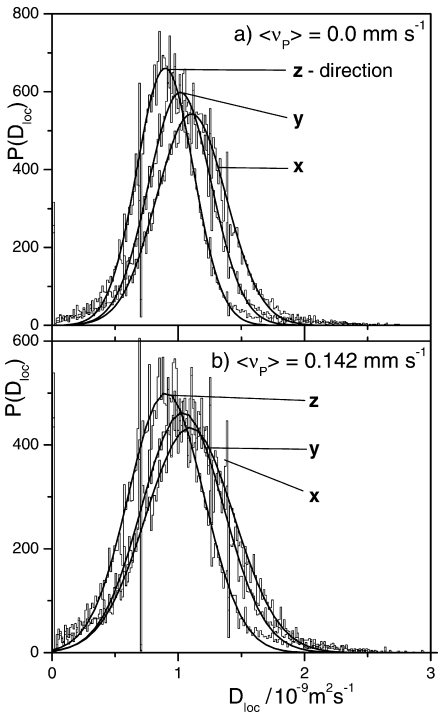

Fig. 10. Local diffusion coefficient frequency distributions for the mixed glass-bead/quartz-sand column. The symbols refer to the spatial coordinates: x (◇), z (□) and transport direction y (△). The curved lines are fits of the normal distribution, for parameters see Table 2. (a) $\langle v_p \rangle = 0.0$ mm s^{-1}, (b) $\langle v_p \rangle = 0.142$ mm s^{-1}.

water cause a dephasing (T_2) of the excited spin states. This dephasing occurs in localized, static magnetic field inhomogeneities and will be rephased partly by the spin-echo sequence (the 180° RF pulse). If the water is now flowing through the porous medium this changes: the mean advective displacement (0.0142 mm) at the highest pore velocity is also of the order of one average pore diameter in 0.1 s and all ^1H_2O molecules will not stay in a localized field gradient but will move over a large distance where they are influenced by a statistical sequence of local gradients. So starting at $v_p = 0$ mm s^{-1} with increasing pore flow velocity, less and less signal is recoverable by the spin-echo pulse and the observed linear dependency of the $\langle \ln I_{b=0} \rangle$ on the mean pore flow velocity in Fig. 9 is obtained.

Switching the diffusion gradients ‘on’, i.e. $b = 1000$ s mm^{-2}, the mean echo intensities decrease not

as strongly as it is the case for the wide-pore glass-bead system (see also Fig. 1). In other words, the difference between the $\langle \ln I_{b=1000} \rangle$ and $\langle \ln I_{b=0} \rangle$ is smaller for all pore velocities. This means that according to Eqs. (1a)–(1c) also the local diffusion coefficients are considerably smaller as for the pure glass-bead system (see Table 2). If one compares the reduction of $\langle D \rangle$ found for bulk water ($2.3 \times 10^{-9}\ m^2\ s^{-1}$) the wide-pore glass-beads system, and the narrow pore system it is clear that the narrow pores restrict the diffusion of water. A similar behavior in the narrow pores was already observed by Schachter et al. (2000), who assigned the decrease of the apparent diffusion coefficient to the restricted pore space.

Finally, Fig. 10 displays the distribution of the obtained local diffusion coefficients for the quartz-sand/glass-beads system. The Gaussian noise is stronger compared to the glass-bead experiment, and even at the greatest mean pore velocity of $v_p = 0.142\ \mathrm{mm\ s^{-1}}$ an asymmetry does not appear, like it has been observed clearly with the glass-bead system. Also an increase of $D_{loc,y}$ with the mean pore water flow velocity could not be observed. Both phenomena could not be explained satisfactorily in this study, they will be subject of a future work. So a flow field could not be calculated and no effective dispersion coefficient could be obtained. But the microscopic Peclet number could be approximated as $p_e \cong 7$, assuming a mean pore diameter of 0.05 mm (see Table 2). This rather small value which would be even much smaller in narrower pores indicates that at least in parts the flux is not dominated by convection but by the local dispersion.

5. General discussion

This work comprises the investigation of the ability of a PGSE imaging sequence for the investigation of hydrodynamic properties of porous media by means of MRI with a conventional medical 1.5T scanner. For this purpose, we have tested two materials of different pore size and heterogeneity: homogeneous 2 mm glass-beads and a heterogeneous mixture of 80% 0.15 mm quartz-sand with 20% of the 2 mm glass-beads. This medium is continuously purged by water at a mean pore velocity ranging from 0 to $0.14\ \mathrm{mm\ s^{-1}}$. The employed PGSE sequence determines local apparent diffusion coefficients of the water flowing through the medium. At zero flow velocity in the wide-pore medium glass-beads, the mean local diffusion coefficient ($\langle D_{loc,y} = 1.9 \times 10^{-9}\ \mathrm{m^2\ s^{-1}}$) is slightly smaller than the ordinary self-diffusion coefficient of pure water. In the fine pore medium, $\langle D_{loc,y} \rangle$ decreases further to about $1.0 \times 10^{-9}\ \mathrm{m^2\ s^{-1}}$. This decrease of the mean local diffusion coefficient reflects the increased restricted diffusion in the narrower pores. This conclusion can be illustrated calculating the mean displacement according to $\langle R \rangle = (6\langle D_{loc,y} \rangle t)^{1/2} = 0.034$ mm for the glass-bead system and 0.025 mm for the glass-bead/quartz-sand mixture, respectively. For the wide-pore system, $\langle R \rangle$ is considerably lower than the mean pore dimension, but gets into the range of the pore dimensions for the fine pore system.

Increasing the pore flow velocity from 0 to $0.14\ \mathrm{mm\ s^{-1}}$ for the glass-bead system a linear increase of $\langle D_{loc} \rangle$ is observable, which is rather weak (10% in this velocity range) for the transverse directions, and slightly greater (20%) for the transport direction. It is caused by mechanical dispersion, i.e. by the small-scale heterogeneity (within the voxel scale) in the flow trajectories, induced by the porous medium. A similar evaluation for the mixed system failed due to a loss of MR signal intensity by frequent wall contacts of the excited water molecules leading to an increased T_2 relaxation. These mean coefficients are termed 'diffusion coefficients', since they reflect mainly the diffusional behavior of the water molecules inside the porous medium, the contribution of the mechanical dispersion in the regarded low pore flow velocity range is rather small as stated in Section 3.1.1. They must not be confused with the effective *dispersion coefficients*, which are valid for the column scale. These coefficients do not correspond to the local diffusion coefficients, but comprise the effects of larger scale heterogeneities on the cm-scale (column scale).

We prove this by a simulation using the particle tracking program PARTRACE, which follows the trajectories of single particles in a given flow field. For this calculation, a divergence free flow velocity fields is necessary, i.e. the continuity equation must be fulfilled. We obtain this by the following procedure: (i) We find that the mean local diffusion coefficients $\langle D_{loc,y} \rangle$ depend linearly on the mean flow velocity

according to Eq. (2) (Pfannkuch, 1963; Roth, 1996). (ii) We assume then that the single local diffusion coefficients $D_{loc,i}$ will also depend linearly on v_p, and (iii) we conclude that the local hydraulic conductivity κ_{loc} is linearly dependent on D_{loc}, assuming a constant pressure gradient. The solving of the Richards equation in three dimensions then yields the 3D flow velocity field, serving as input for PARTRACE. This is performed by means of the program TRACE with the additional boundary condition that the mean flux must correspond to the mean applied flow rate.

This simulation reflects the existence of tubular like structures in one half of the column, where the diffusivity is enhanced (Figs. 3 and 7). In these structures, the enhanced hydraulic conductivity leads to an increased transport velocity of the tracer. These structures probably result from packing errors, which exist, as can bee seen from the total water content of $\theta = 0.4$, whereas the free volume of an ideal packing of spheres is 0.26. It should be noted here that the slightly enhanced mobility in these regions must not be confused with the strongly enhanced flow velocities, occurring, e.g. in very localized flow paths in fractured systems (Berkowitz and Scher, 1998). In such systems, the high-flow velocities (0.3–1.5 mm s^{-1}) can be monitored by specialized, velocity sensitive spin-echo MRI sequences (Dijk et al 1999; Dijk and Berkowitz, 1999).

From the concentration distribution of the tracer in the column at given times, the effective dispersion coefficient for the glass-bead column is obtained by plotting the second spatial moment of this distribution versus time. After an initial period of about 25 min, corresponding to a pore flow distance of 6 cm, the macroscopic effective dispersion coefficient is established as $D_{eff} = 130 \times 10^{-9}$ m^2 s^{-1}, which coincides very well with an experimentally measured value of 93×10^{-9} m^2 s^{-1}, obtained from the Ni^{2+} motion through a glass-bead porous system (Herrmann et al., 2002). This high value directly results from the existence of the areas of higher permittivity, found by the 3D measurement of the local diffusion coefficients. This proves that the observed very large difference between the local diffusion coefficient and the macroscopic dispersion coefficient (factor 68) is not due to additive effects of the local mechanical dispersion but is caused by macroscopic heterogeneities (packing errors).

Summarizing this work, it can be stated that MRI with a conventional medical scanner, employing a PGSE sequence, and applied to the study of hydrodynamic properties of porous media, is a valuable technique for the understanding of transport properties. The method is very convenient for the study of coarse pore systems, where the mean diffusional plus advectional displacement of the water molecules is sufficiently smaller than the mean pore size. The mean diffusional displacement may be estimated by $\langle R \rangle = (6Dt)^{1/2}$, and the mean advectional displacement from the pore velocity. The time t is given by the echo time of the PGSE sequence (see Eqs. (1a)–(1c)). Further limitations are the gradient strengths and the low (compared to dedicated MRI scanners for small volumes) main magnetic field. Especially, a higher main magnetic field would result a better signal to noise ratio, which combined with stronger and faster magnetic gradients would allow more exact velocity fields and a higher resolution. However, we could demonstrate that the accuracy of the data is good enough for further statistical analyses. The method works well for systems with coarse pore sizes. For narrower pore sizes, the approach is of rather limited value since the increased number of wall contacts leads to an increased T_2 relaxation. Here, other specialized sequences would be preferable.

Acknowledgments

The authors thank Dr Hans-Jörg Wittsack and E. Rädisch, MRI Department of the University Hospital Düsseldorf, Germany for assistance with the measurements on the local Siemens 1.5 T scanner.

References

Baumann, T., Petsch, R., Niessner, R., 2000. Direct 3D measurement of the flow velocity in porous media using magnetic resonance tomography. Environ. Sci. Technol. 34, 4242–4248.

Berkowitz, B., Scher, H., 1998. Theory of anomalous chemical transport in random fracture networks. Phys. Rev. E. 57, 5858–5869.

Callaghan, P.T., 1991. Principles of Nuclear Magnetic Resonance Microscopy, Oxford University Press, Oxford, UK.

De Marsily, G., 1986. Quantitative Hydrogeology, Academic Press, New York.

De Panfilis, C., Packer, K.J., 1999. Characterisation of porous media by NMR imaging and flow-diffraction. Eur. Phys. J. Appl. Phys. 8, 77–86.

Deutsch, C.V., Journel, A.G., 1992. GSLIB: Geostatistical Software Library and User's Guide, Oxford University Press, Oxford, UK.

Dijk, P.E., Berkowitz, B., 1999. Three-dimensional flow measurements in rock fractures. Wat. Resour. Res. 35, 3955–3959.

Dijk, P.E., Berkowitz, B., Bendel, P., 1999. Investigation of flow in water-saturated rock fractures using nuclear magnetic resonance imaging (NMRI). Wat. Resour. Res. 35, 347–360.

Freyberg, D.L., 1986. A natural gradient experiment on solute transport in a sand aquifer. 2. Spatial moments and the advection and dispersion of non-reactive tracers. Wat. Resour. Res. 22, 2031–2046.

Gembris, D., 2001. Rekonstruktion neuronaler Konnektivität mittels kernmagnetischer Resonanz (Reconstruction of neural connectivity using nuclear magnetic resonance). Thesis, University Dortmund, Germany, http://eldorado.uni-dortmund.de:8080/FB2/ls3/forschung/2001/Gembris.

Grenier, A., Schreiber, W., Brix, G., Kinzelbach, W., 1997. Magnetic resonance imaging of paramagnetic tracers in porous media: quantification of flow and transport parameters. Wat. Resour. Res. 33, 1461–1473.

Herrmann, K.-H., 2001. Nichtinvasive Charakterisierung von Transporteigenschaften poröser Medien: Dreidimensionale Untersuchungen mit Hilfe der Kernspintomographie (Non-invasive characterization of transport properties of porous media: three-dimensional investigations using nuclear magnetic resonance tomography). Thesis, University Bonn, Germany.

Herrmann, K.-H., Pohlmeier, A., Wiese, S., Shah, N.J., Nitzsche, O., Vereecken, H., 2002. Three dimensional Ni^{2+} ion transport through porous media using magnetic resonance imaging (MRI). J. Environ. Qual. in press.

Landold-Börnstein, 1969, Sixth ed, Zahlenwerte und Funktionen aus Physik, Chemie, Astronomie, Geophysik und Technik, vol. II5a. Springer, Berlin.

Manz, B., Alexander, P., Gladden, L.F., 1999. Correlations between dispersion and structure in porous media probed by nuclear magnetic resonance. Phys. Fluids 11, 259–267.

Neuendorf, O., 1997. Numerische 3D simulation des stofftransports in einem heterogenen aquifer (Numerical 3D simulation of solute transport in a heterogeneous aquifer). Thesis, Research Centre Jülich Publication, Jülich, Germany.

Oswald, S., Kinzelbach, W., Greiner, A., Brix, G., 1997. Observation of flow and transport processes in artificial porous media via magnetic resonance imaging in three dimensions. Geoderma 80, 417–429.

Pfannkuch, H.O., 1963. Contribution à l'étude des déplacements des fluides miscible dans un milieu poreux. Rev. Inst. Fr. Petrol. 18, 215–270.

Roth, K., 1996. Lecture notes in soil physics. http://www.uphys.uni-heidelberg.de/ts/students/sp3.html, University Heidelberg, Germany.

Schachter, M., Does, M.D., Anderson, A.W., Gore, J.C., 2000. Measurements of restricted diffusion using an oscillating gradient spin-echo sequence. J. Magn. Res. 147, 232–237.

Scheenen, T.W.J., Vergeldt, F.J., Windt, C.W., de Jaeger, P.A., Van As, H., 2001. Microscopic imaging of slow flow and diffusion: a pulsed gradient stimulated echo sequence combined with turbo spin-echo imaging. J. Magn. Res. 151, 94–100.

Sederman, A.J., Gladden, L.F., 2001. Magnetic resonance visualization of single- and two-phase flow in porous media. Magn. Res. Imag. 19, 229–343.

Seidemann, R.W., 1997. Untersuchungen zum Transport von gelösten Stoffen und Partikeln durch heterogene Porengrundwasserleiter (Investigations on solute and particle transport through heterogeneously porous aquifers), Research Center Jülich Publication, Jülich, Germany.

Watson, A.T., Chang, C.T.P., 1997. Characterizing porous media with NMR methods. Prog. Nucl. Magn. Reson. Spectrosc. 31, 343–386.

Zhong, J., Kennan, R.P., Gore, J.C., 1991. Effects of susceptibility variations on NMR measurements of diffusion. J. Magn. Res. 95, 267–280.